ISSN 1990-7931, Russian Journal of Physical Chemistry B, 2025, Vol. 19, No. 2, pp. 319–335. © Pleiades Publishing, Ltd., 2025.

STRUCTURE OF CHEMICAL COMPOUNDS, QUANTUM CHEMISTRY, SPECTROSCOPY

Divulge of Hydrogen Energy Storage by Manganese Doped Nitrogen Nanocomposites of Aluminum, Gallium or Indium Nitrides: A First-Principles Study

F. Mollaamin[a], * and M. Monajjemi[b]

[a] *Department of Biomedical Engineering, Faculty of Engineering and Architecture, Kastamonu University, Kastamonu, Turkey*
[b] *Department of Chemical Engineering, Central Tehran Branch, Islamic Azad University, Tehran, Iran*
** e-mail: fmollaamin@kastamonu.edu.tr*

Received October 22, 2024; revised November 18, 2024; accepted November 20, 2024

Abstract—This work studied the Mn dopant layer gallium nitride (GaN) and addressed the suitability of Mn-doping as a means to potentially produce a semiconductor material system in GN derivatives. A comprehensive investigation on hydrogen grabbing by heteroclusters of Mn-doped GaN, AlGaN, InGaN was carried out using DFT computations at the CAM–B3LYP–D3/6–311+G(*d*, *p*) level of theory. The notable fragile signal intensity close to the parallel edge of the nanocluster sample might be owing to manganese binding induced non-spherical distribution of Mn@GaN, Mn@AlGaN or Mn@InGaN heteroclusters. The hypothesis of the energy adsorption phenomenon was confirmed by density distributions of CDD, TDOS/PDOS/OPDOS, and ELF for GaN and its alloys. A vaster jointed area engaged by an isosurface map for Mn doping GaN, AlGaN, InGaN towards formation of nanocomposites of Mn@GaN–H, Mn@AlGaN–H, Mn@InGaN–H after hydrogen adsorption due to labeling atoms of N4, Mn5, H18, respectively. Therefore, it can be considered that manganese in the functionalized Mn@GaN, Mn@AlGaN or Mn@InGaN might have more impressive sensitivity for accepting the electrons in the process of hydrogen adsorption. The changes of Gibbs free energy versus for all nanocomposites could detect the maximum efficiency of Mn@AlGaN–H > Mn@GaN–H > Mn@InGaN–H for energy storage through ΔG_f^o. The advantages of manganese over GaN, AlGaN, or InGaN include its higher electron and hole mobility, allowing manganese doping devices to operate at higher frequencies than non-doping devices.

Keywords: semiconductor, hydrogen adsorption, energy storage, aluminum gallium nitride, indium gallium nitride, first-principles study

DOI: 10.1134/S199079312570006X

1. INTRODUCTION

Exploring energy storage materials with ultralong cycle lifespan and high energy/power density in extremely high-temperature environments is crucial [1–7]. A few-layered GaN crystal rich in N-vacancies is designed and fabricated via an efficient and facile strategy, which further increases its specific area and active sites. Additionally, the energy storage mechanism of GaN with N vacancies is further investigated using density functional theory calculations [8–15]. Ternary "AlGaN" alloys have been recognized as promising materials for realizing deep ultraviolet "DUV" optoelectronic devices with operating wavelengths down to 200 nm [16–18]. For the development of high performance AlGaN-based "DUV" devices, high-conductivity *p*-type Al-rich $Al_xGa_{1-x}N$ ($x \geq 0.4$) is essential. Many studies have shown that enhancing the *p*-type conductivity has a significant effect on the improvement of both the electrical and optical properties of AlGaN DUV optoelectronics [19–23]. In an investigation, the scientists have shown the $Al_{0.1}Ga_{0.9}N$/GaN heterojunction solar cells with a Mn-doped active layer. Under a 1-sun AM1.5 G illumination condition, the devices exhibited an improved conversion efficiency by a magnitude of 5 compared to the cells without Mn doping in the active layer. This dramatic increase in conversion efficiency is attributed to the fact that the Mn-related energy states cause sub-band gap photon absorption and thereby contribute an extra photocurrent [24–26]. The investigations conducted on Mn-doped GaN have shown that the Mn impurity band could form approximately at the middle of the GaN band gap [27].

The researchers have estimated the suitability of Mn doped $In_{1-x}Ga_xN$ as an IB material. They predicted that the $In_{1-x}Ga_xN$-based solar cells with an Mn-doped absorption layer could achieve maximum efficiency [28, 29]. The ternary semiconductor of Indium gallium nitride (InGaN) as solar cells is remarkable owing to the adjustable direct band gap

energy of InGaN veiling the total solar spectrum arraying from 0.7 to 3.4 eV [30, 31], as well as preferable photovoltaic specifics of InGaN consisting of vast absorption coefficients [32] and high carrier dynamism. Furthermore, great fixity and excellent radiation persistence of InGaN alloys permit function of InGaN-based instruments in uttermost situations such as space and geocentric usages [30, 33]. The solar cells of InGaN were constructed with low indium amounts of the InGaN alloy compounds [34–36] which conduces to an enhancement in the band gap energy of InGaN and then eventuates in the absorption of shorter wavelengths of solar radiation. Therefore, to find out InGaN solar cells with high yield, the In amount in the InGaN active layer of these solar cells should be enhanced to compensate a large part of the solar spectrum. Recently, it has been suggested the application of dual nanogratings of Si and other organic solar cells which are mostly in direct contact with the active area of the solar cells [37–43]. Moreover, the researchers fabricated transition metal zinc doped InGaN nanorods arrays by radio-frequency plasma-assisted molecular beam epitaxy. Doping obviously reduces indium atoms composition, the aggregation of In–In and induces the deep energy level. This greatly decreases the defects and improves the valence band potential of InGaN nanorods [44]. Recently, researchers have proposed an InGaN/GaN *p–i–n* thin-film solar cell which includes a dual nanograting compound: silver nanogratings on the back of the solar cell and GaN–NGs on the front. FDTD simulation parameters have exhibited that the dual NG compound connects the eventual sunlight to the plasmonic and photonic styles, so enhancing the absorption of the solar cell in a wide spectral span. It is perceived that the solar cells possessing the double nanograting structures have a considerable increment in light absorption compared with cells having either no nanogratings or having only the front nanogratings or only the back nanogratings [45, 46].

Particularly, the Mn incorporation was found to drop off precipitously with increasing Ga-rich conditions. Furthermore, there have been indications of $GaMn_3N$ clusters precipitating under stoichiometric conditions for Mn concentrations more than a couple of percent [47]. To try to avoid this type of problem and alongside the developing effort studying Mn-doping of GaN, many other semiconducting host materials have been investigated including silicon germanium, gallium phosphide, silicon carbide, and zinc oxide just to name a few, to realize a room temperature DMS material without second-phase precipitation [48]. Moreover, many different dopant species, both transition metal and rare earth, have also been tried [49].

In this paper, we propose the feasible semiconductors of GaN, AlGaN, InGaN which are doped with manganese. We carried out molecular modelling considering the geometrical parameters of doping atoms on the surface of Mn@GaN, Mn@AlGaN, Mn@InGaN through hydrogen absorption status and current charge density was studied. Moreover, the effect of a relative chemical shift between GaN, AlGaN, InGaN and doped heteroclusters was also investigated. This study systematically demonstrates the application potential of GaN crystals and provides a strategy for the application of wide-bandgap semiconductors in a new field.

2. THEORY, MATERIALS AND COMPUTATION

The Mn-doped GaN, AlGaN, InGaN nanocomposites were calculated within the framework of first-principles calculation based on density functional theory (DFT) (Fig. 1). The rigid potential energy surface using density functional theory [50–60] was performed due to Gaussian 16 revision C.01 program package [61] and GaussView 6.1 [62]. The coordination input for energy storage has applied 6–311+G(*d*, *p*) and EPR–3 basis sets.

First, we optimized the structural parameters of nanoclusters of GaN, AlGaN, InGaN which are doped with manganese towards formation of heteroclusters of Mn@GaN, Mn@AlGaN, Mn@InGaN for obtaining the highest short-circuit current density. Then, Fig. 1 shows the process of hydrogen adsorption on heteroclusters of Mn@GaN, Mn@AlGaN, Mn@InGaN which are varied to maximize the absorption in the active region. This is a utility used to calculate ring area and perimeter, since ring area is sometimes involved in wavefunction analysis. In this function, it is needed to input the index of the atoms in the ring in clockwise manner including Mn5, N4, Ga15, N7, Ga6, N12 (Figs. 1a–1c). Then, it has been calculated total ring area and total ring perimeter for a tailored ring as 9.6981 and 11.6921 $Å^2$, respectively (Figs. 1a–1c).

3. RESULTS AND DISCUSSION

In this article, the data has evaluated the efficiency of metal-doped hybrid nanoalloys of Mn@GaN, Mn@AlGaN, Mn@InGaN and their hydrated complexes of Mn@GaN–H, Mn@AGaN–H, Mn@InGaN–H energy-saving in batteries, transistors and solar cells.

3.1. Analysis of CDD, TDOS/PDOS/OPDOS and ELF

The amounts of charge density differences "CDD" is measured by considering isolated atoms or noninteracting ones. The mentioned approximation can be the lightest to use because the superposition value may be received from the primary status of the self-consistency cycle in the code that carries out the density functional theory (Figs. 2a–2c) [63]. Figure 3a indicates the atom of Mn5 from Mn@GaN and Mn5, H18 from Mn@GaN–H accompanying gallium and nitrogen atoms fluctuating around –9 to +3 Bohr. In Fig. 3b,

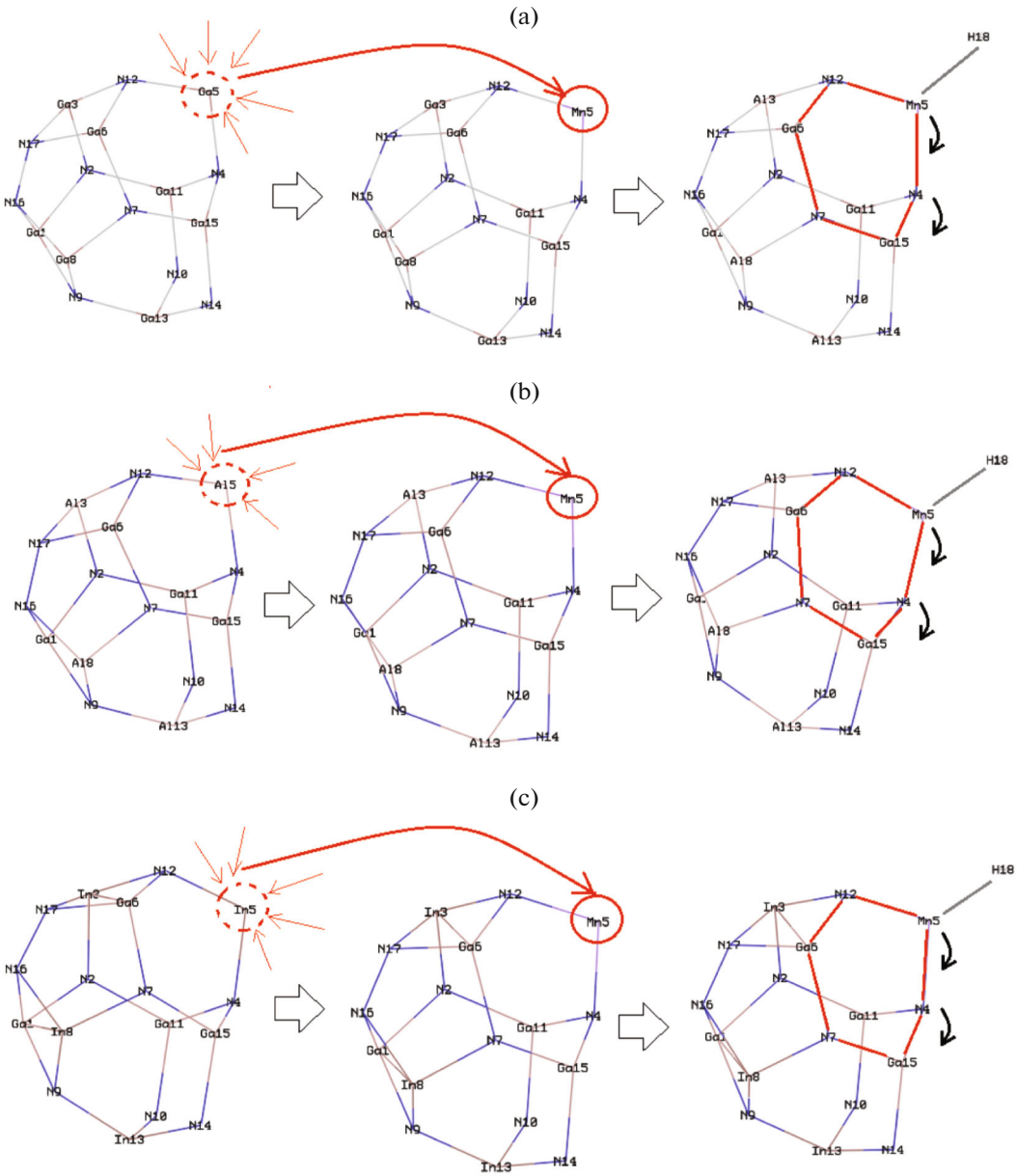

Fig. 1. Characterization of heteroclusters include (a) Mn@GaN/Mn@GaN–H, (b) Mn@AlGaN/Mn@AlGaN–H, (c) Mn@InGaN/Mn@InGaN–H through a labeled ring in clockwise manner including Mn5, N4, Ga15, N7, Ga6, N12 towards H-adsorption.

the atom of Mn5 from Mn@AlGaN and Mn5, H18 from Mn@AlGaN–H accompanying aluminum, gallium and nitrogen atoms have shown the fluctuation around –9 to +3 Bohr and –8 to +4 Bohr, respectively. Moreover, the atom of Mn5 from Mn@InGaN and Mn5, H18 from Mn@InGaN–H accompanying indium, gallium and nitrogen atoms have shown the fluctuation around –9 to +3 Bohr (Fig. 2c).

To better understand the different adsorption characteristics of Mn@GaN, Mn@GaN–H, Mn@AlGaN, Mn@AlGaN–H, Mn@InGaN, Mn@InGaN–H, total density of states (TDOS) using Multiwfn program [64] has been measured. This parameter can indicate the existence of important chemical interactions often on the convex side (Figs. 3a, 3a', 3b, 3b', 3c, 3c'). In isolated system (such as molecule), the energy levels are discrete, the concept of density of state (DOS) is supposed completely valueless in this situation. Therefore, the original total DOS (TDOS) of isolated system can be written as [64]:

$$\mathrm{TDOS}(E) = \sum_i \delta(E - \epsilon_i). \quad (1)$$

The normalized Gaussian function is defined as:

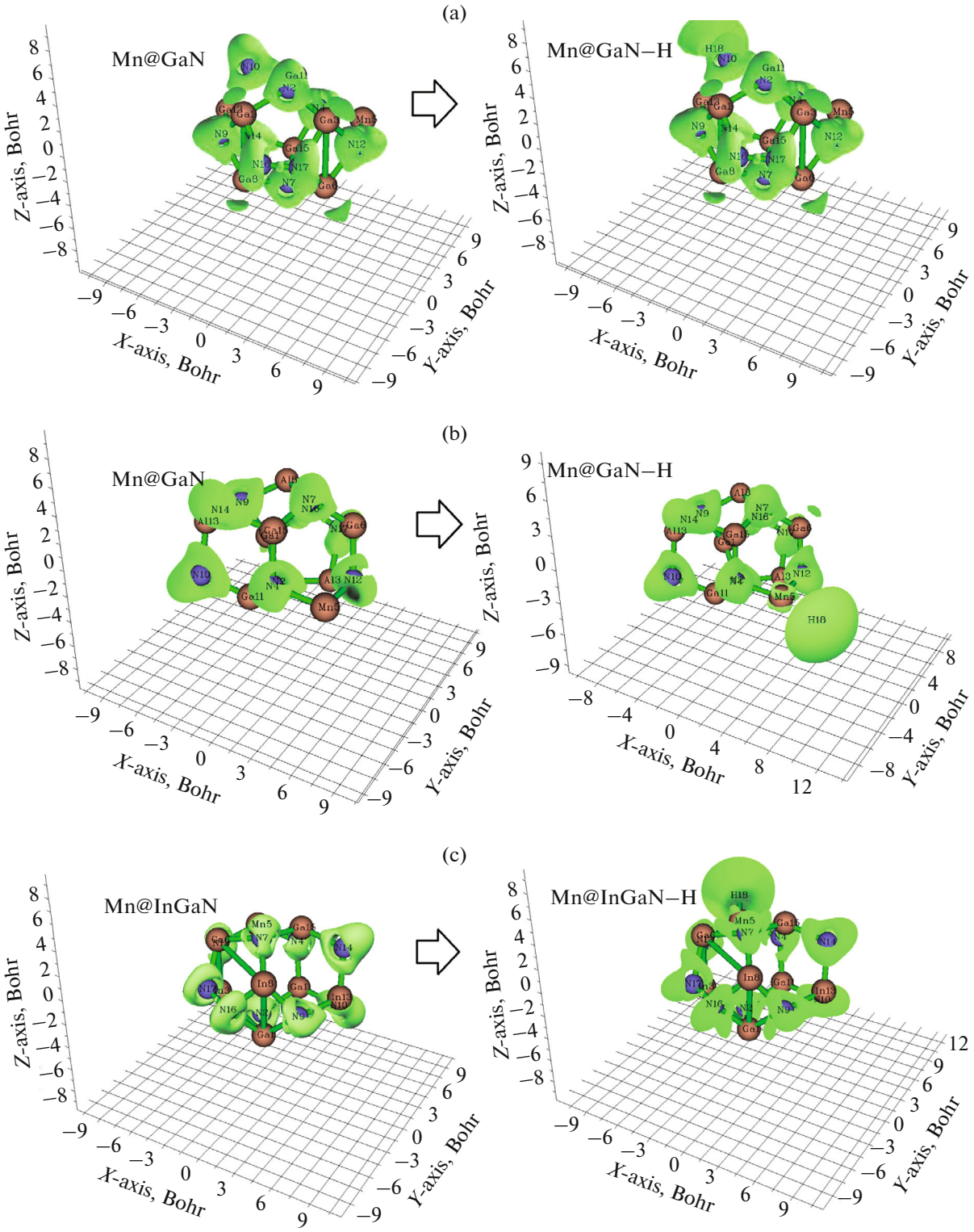

Fig. 2. CDD graphs for heteroclusters through hydrogen adsorption including (a) Mn@GaN/Mn@GaN–H, (b) Mn@AlGaN/Mn@AlGaN–H, and (c) Mn@InGaN/Mn@InGaN–H.

$$G(x) = \frac{1}{c\sqrt{2\pi}} e^{-\frac{x^2}{2c^2}} \text{ where } c = \frac{\text{FWHM}}{2\sqrt{2\ln x}}. \quad (2)$$

FWHM (full width at half maximum) is an adjustable parameter in Multiwfn. Moreover, the curve map of broadened partial DOS (PDOS) and overlap DOS

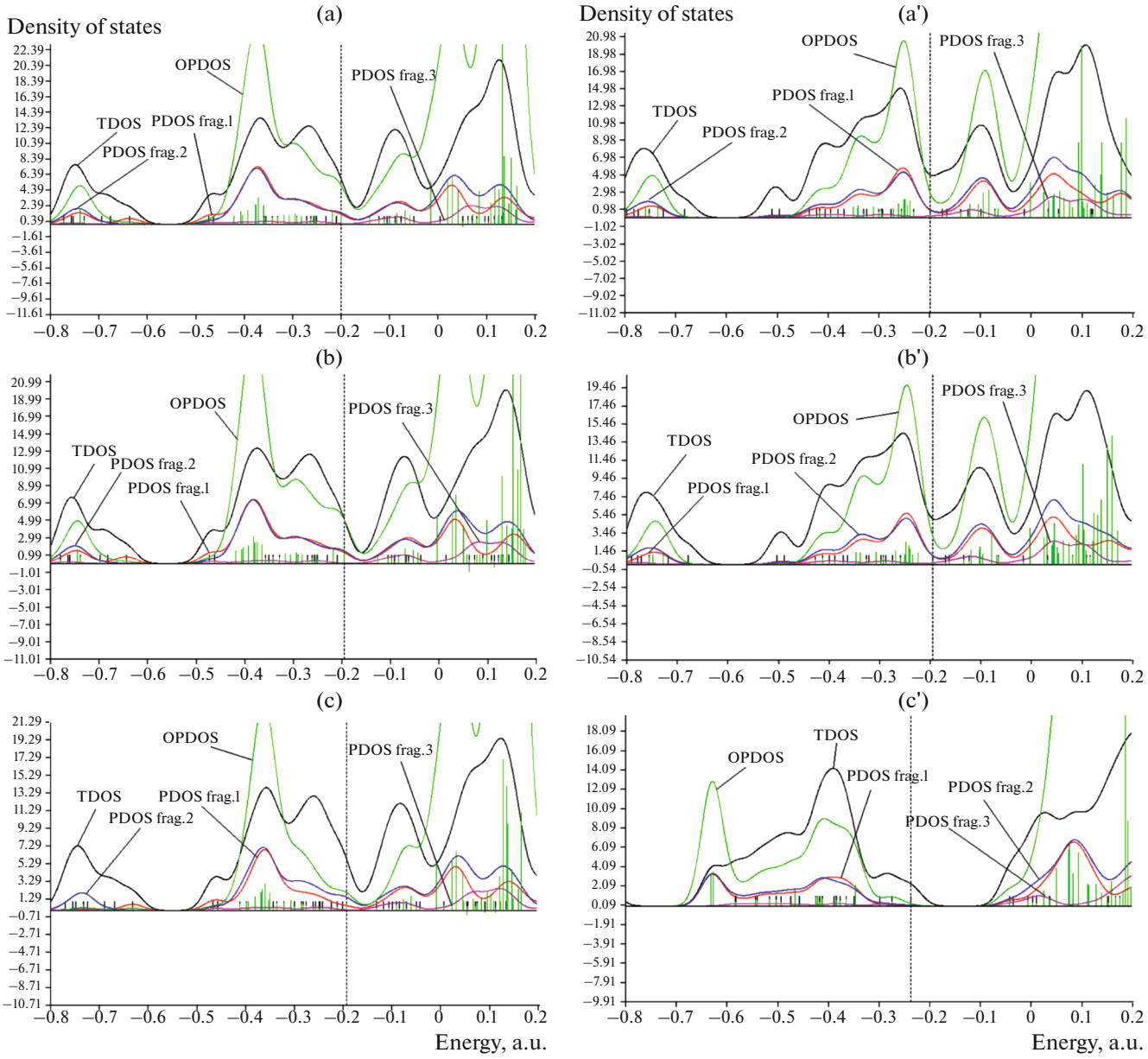

Fig. 3. TDOS/PDOS/OPDOS graphs of heteroclusters include (a) Mn@GaN, (a') Mn@GaN–H, (b) Mn@AlGaN, (b') Mn@AlGaN–H, (c) Mn@InGaN, (c') Mn@InGaN–H.

(OPDOS) are valuable for visualizing orbital composition analysis, PDOS function of fragment A is defined as:

$$\mathrm{PDOS}_A(E) = \sum_i \Xi_{i,A} F(E - \epsilon_i), \qquad (3)$$

where $\Xi_{i,A}$ is the composition of fragment A in orbital i. The OPDOS between fragment A and B is defined as:

$$\mathrm{OPDOS}_{A,B}(E) = \sum_i \mathrm{X}^i_{A,B} F(E - \epsilon_i), \qquad (4)$$

where $\mathrm{X}^i_{A,B}$ is the composition of total cross term between fragment A and B in orbital i.

In the TDOS map, each discrete vertical line corresponds to a molecular orbital (MO), the dashed line highlights the position of HOMO. The curve is the TDOS simulated based on the distribution of MO energy levels. In the negative part, the region around −0.40 a.u. has obviously larger state density than other regions for Mn@GaN, Mn@GaN–H, Mn@AlGaN, Mn@AlGaN–H, Mn@InGaN, Mn@InGaN–H (Figs. 3a, 3a', 3b, 3b', 3c, 3c'). However, Mn@InGaN–H (Fig. 3c') has shown larger state density through pointed peaks than Mn@GaN–H (Fig. 3a') and Mn@AlGaN–H (Fig. 3b'). It is remarkable that the excessive growth technique on doping manganese as noble transition metal is a potential approach to

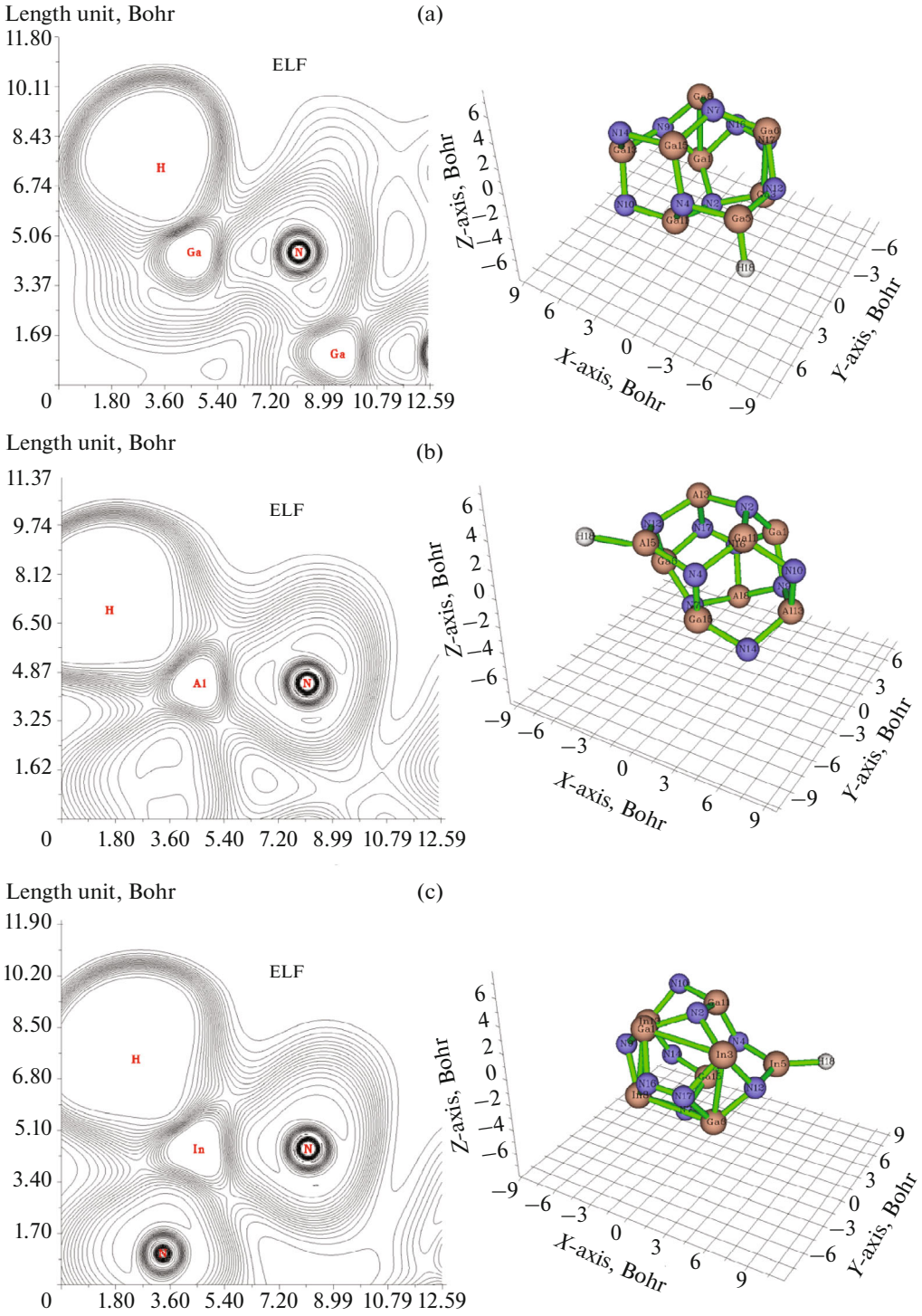

Fig. 4. The counter line maps of ELF for heteroclusters include (a) GaN–H, (b) AlGaN–H, and (c) InGaN–H.

designing high efficiency hybrid semipolar gallium nitride alloys devices on aluminum or indium layers in a long wavelength zone.

Fragment 1 has been defined for N2, X3 (X = Ga, Al, In), N4, Mn5, Ga11, N12, N17 for Mn@GaN (Fig. 3a), Mn@AlGaN (Fig. 3b), Mn@InGaN (Fig. 3c) and H18 for Mn@GaN (Fig. 3a'), Mn@AlGaN (Fig. 3b'), Mn@InGaN (Fig. 3c'). Moreover, Fragment 2 has indicated the fluctuation of N4, Mn5, Ga6, N10, N12, Y13 (Y = Ga, Al, In), Ga15, N17 for Mn@GaN (Fig. 3a), Mn@AlGaN (Fig. 3b), Mn@InGaN (Fig. 3c) and H18 for Mn@GaN (Fig. 3a'), Mn@AlGaN (Fig. 3b'),

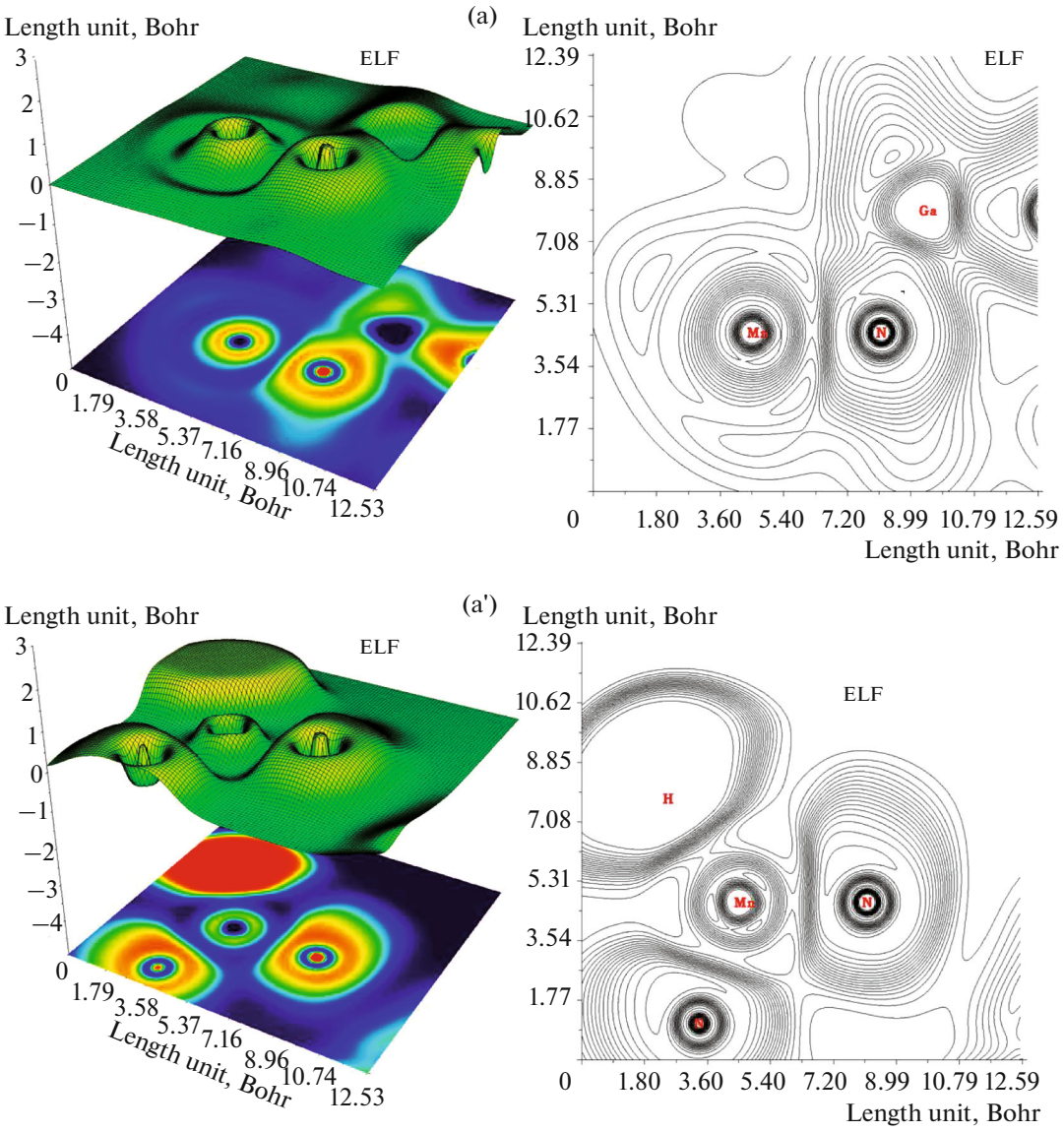

Fig. 5. The graphs of ELF for heteroclusters include (a) Mn@GaN/Mn@GaN–H, (b) Mn@AlGaN/Mn@AlGaN–H, and (c) Mn@InGaN/Mn@InGaN–H (Counter line map in the right and shaded surface map with projection in the left).

Mn@InGaN (Fig. 3c'). Finally, it was considered the fluctuation of Ga1, N7, Z8 (Z = Ga, Al, In), N9, Y13 (Y = Ga, Al, In), 14, 16, N17 for Mn@GaN (Fig. 3a), Mn@AlGaN (Fig. 3b), Mn@InGaN (Fig. 3c) and H18 for Mn@GaN (Fig. 3a'), Mn@AlGaN (Fig. 3b'), Mn@InGaN (Fig. 3c') through Fragment 3.

Furthermore, a type of scalar fields called electron localization function (ELF) may demonstrate a broad span of bonding samples. Nevertheless, the distinction between deduced/raised electron delocalization/localization into cyclic π-conjugated sets stays encouraging for ELF [65]. The grosser the electron localization is in an area, the more likely the electron movement is restricted within it. Therefore, they might be discerned from the ones away if electrons are totally centralized. As Bader investigated, the zones with large electron localization possess extensive magnitudes of Fermi hole integration. But, with having a six-dimension function for the Fermi hole, it seems hard to be studied directly. Then, Becke and Edgecombe remarked that spherically averaged like spin conditional pair probability possesses a direct correlation with the Fermi hole and proposed the parameter of electron localization function (ELF) in Multiwfn program [64] and popularized for spin-polarized procedure [66]:

$$\mathrm{ELF}(r) = \frac{1}{1 + [D(r)/D_0(r)]}, \tag{5}$$

where

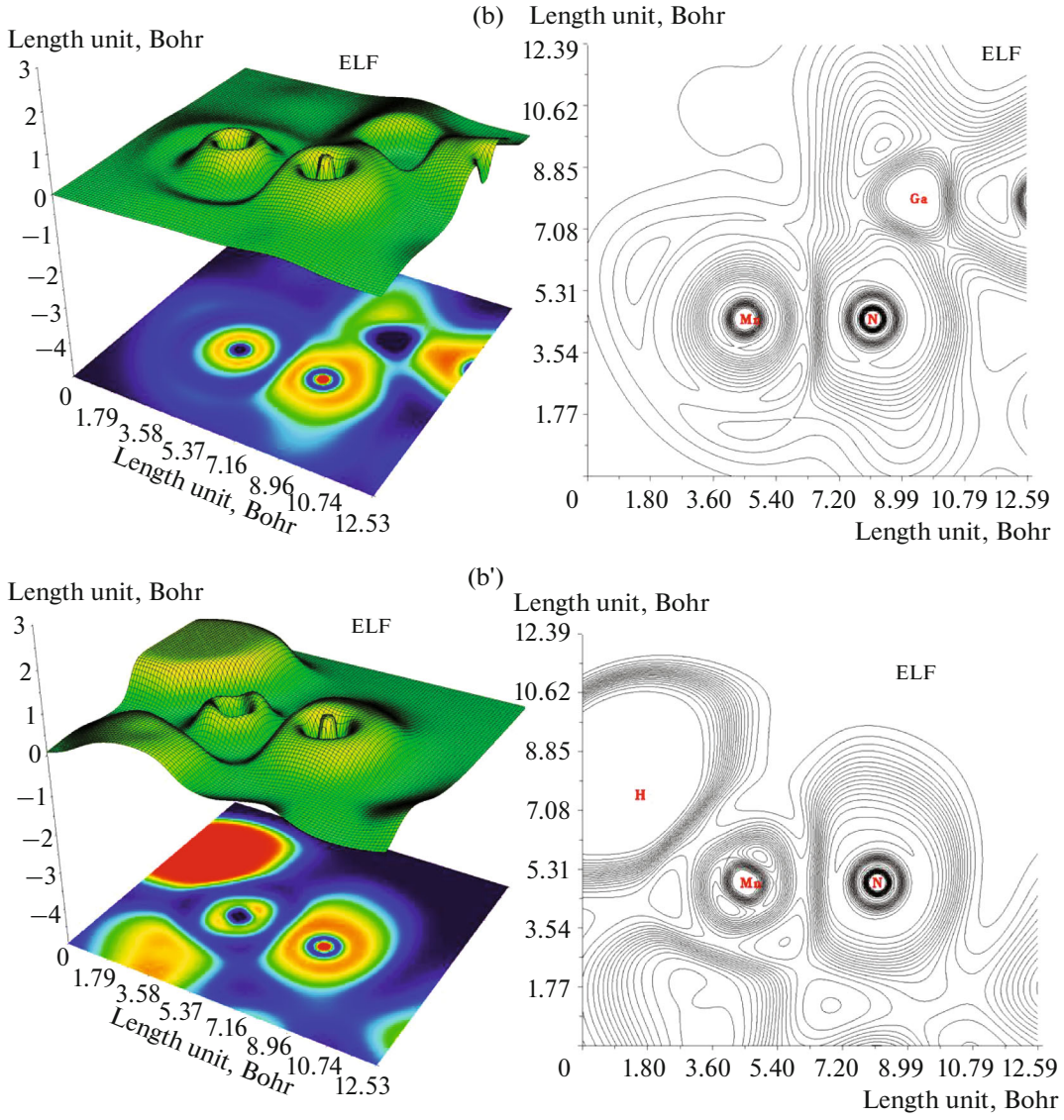

Fig. 5. (Contd.)

$$D(r) = \frac{1}{2}\sum_i \eta_i |\nabla\varphi_i(r)|^2 - \frac{1}{8}\left[\frac{|\nabla\rho_\alpha(r)|^2}{\rho_\alpha(r)} + \frac{|\nabla\rho_\beta(r)|^2}{\rho_\beta(r)}\right], \quad (6)$$

and

$$D_0(r) = \frac{3}{10}\left(6\pi^2\right)^{2/3}\left[\rho_\alpha(r)^{5/3} + \rho_\beta(r)^{5/3}\right]. \quad (7)$$

For close-shell system, since $\rho_\alpha = \rho_\beta = (1/2)\rho$, D and D_0 terms can be simplified as:

$$D(r) = \frac{1}{2}\sum_i \eta_i |\nabla\varphi_i(r)|^2 - \frac{1}{8}\frac{|\nabla\rho(r)|^2}{\rho(r)}, \quad (8)$$

and

$$D_0(r) = (3/10)\left(3\pi^2\right)^{2/3}\rho(r)^{5/3}. \quad (9)$$

Regarding kinetic energy, ELF was rechecked to be more punctual for both Kohn–Sham DFT and post-HF wavefunctions [67]. In fact, the excess kinetic energy density caused by Pauli repulsion was unfolded by $D(r)$ and $D_0(r)$ may be inspected as Thomas–Fermi kinetic energy density. Because $D_0(r)$ is brough forward the ELF as origin, what the ELF shows is an affiliate localization. Regarding hydrogen adsorption, the complexes of GaN–H, AlGaN–H, and InGaN–H can be defined by ELF graphs owing to exploring their delocalization/localization characterizations of electrons and chemical bonds (Figs. 4a–4c). After Mn-doping, the counter map of ELF for Mn@GaN, Mn@GaN–H (Figs. 5a, 5a'), Mn@AlGaN, Mn@AlGaN–H (Figs. 5b, 5b'), Mn@InGaN, Mn@InGaN–H (Figs. 5c, 5c') has shown the electron delocalization through a labeled ring in clockwise

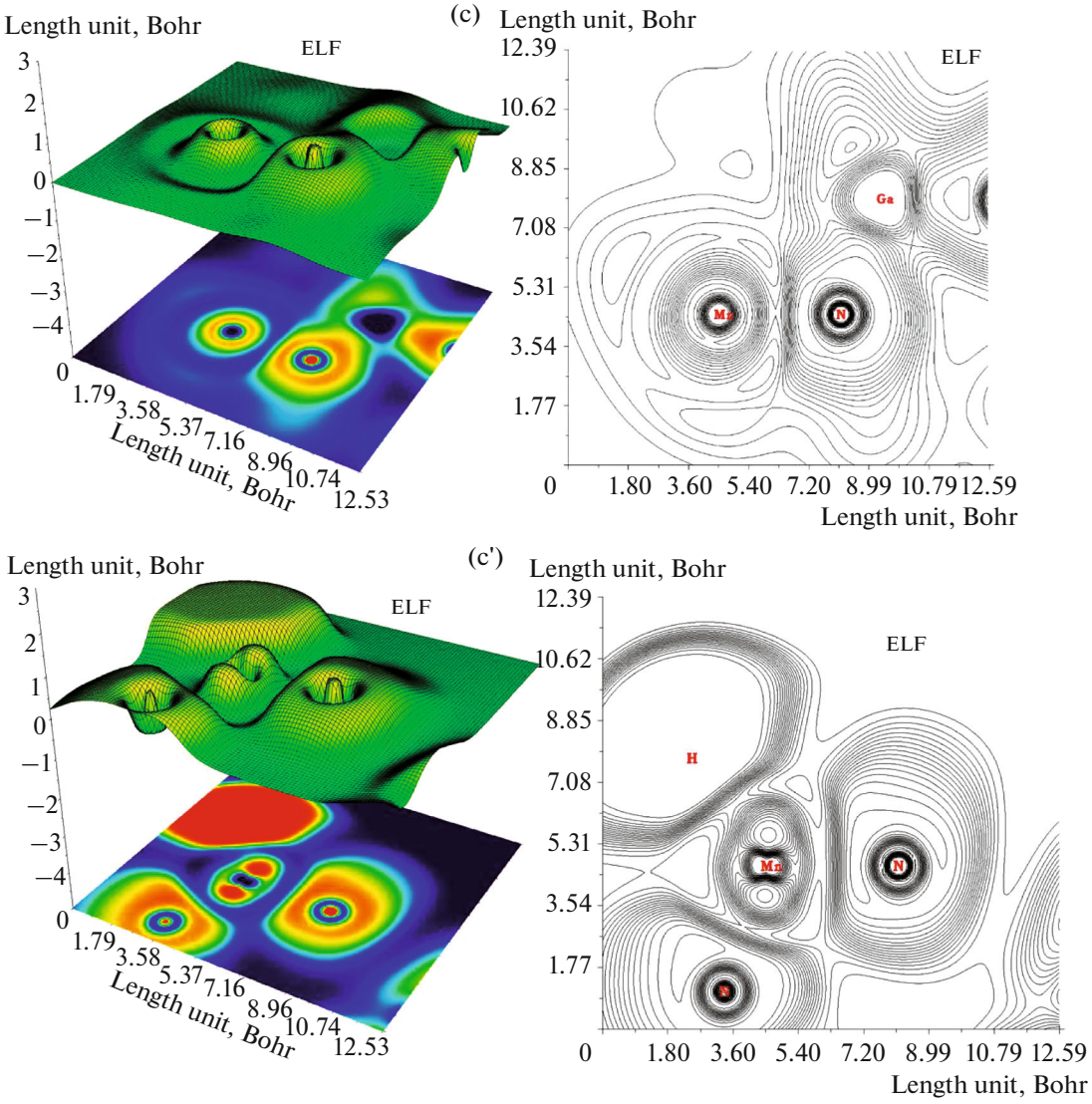

Fig. 5. (Contd.)

manner including Mn5, N4, Ga15, N7, Ga6, N12 and H18 towards H-adsorption (Figs. 1a–1c). Then, hydration of Mn-doped GaN, AlGaN, InGaN indicates a larger isosurface map of electron delocalization due to labeling atoms of N4, Mn5, H18 in Mn@GaN–H (Fig. 5a'), Mn@AlGaN–H (Fig. 5b'), Mn@InGaN–H (Fig. 5c'). A narrower connected area occupied by an isosurface map means that electron delocalization is relatively difficult. However, the large counter map of ELF for Mn@GaN, Mn@AlGaN, Mn@InGaN can confirm that doping Mn nanoparticles on the surface increases the efficiency of GaN, AlGaN, InGaN for energy storage (Table 1).

Besides, the changes of charge density analysis have illustrated that GaN, AlGaN, InGaN have shown the Bader charge of −1.092, −1.272, −1.131 coulomb before Mn-doping and −1.048, −1.252, −1.098 coulomb after Mn-doping respectively, that describes the tensity value of these heteroclusters for energy storage (Table 1).

3.2. Analysis of Nuclear Magnetic Resonance Spectra

The successful formation of Mn-doped GaN layers suggests the need for investigations of magnetic properties to explore possibilities for developing GaN-based spintronic devices. Based on the resulted amounts, nuclear magnetic resonance (NMR) spectra of Mn@GaN, Mn@AlGaN, Mn@InGaN heteroclusters as the potential molecules for energy storage can unravel the efficiency of these complexes through hydrogen adsorption [68–83]. From the DFT calculations, it has been attained the chemical shielding (CS) tensors in the principal axes system to estimate the iso-

Table 1. Data of Bader charge (Q/Coulomb) for selected atoms of Mn@GaN, Mn@GaN–H, Mn@AlGaN, Mn@AlGaN–H, Mn@InGaN, Mn@InGaN–H heteroclusters

Mn@GaN		Mn@GaN–H		Mn@AlGaN		Mn@AlGaN–H		Mn@InGaN		Mn@InGaN–H	
atom	*Q*	atom	Q	atom	Q	atom	Q	atom	Q	atom	Q
Ga1	0.99	Ga1	1.01	Ga1	0.98	Ga1	0.99	Ga1	0.95	Ga1	1.31
N2	−1.05	N2	−1.04	N2	−1.15	N2	−1.13	N2	−1.06	N2	−1.45
Ga3	0.97	Ga3	0.99	Al3	1.25	Al3	1.25	In3	1.08	In3	1.48
N4	−1.01	N4	−0.92	N4	−1.05	N4	−0.94	N4	−1.02	N4	−1.34
Mn5	0.75	Mn5	0.42	Mn5	0.76	Mn5	0.39	Mn5	0.72	Mn5	0.81
Ga6	0.97	Ga6	0.99	Ga6	0.97	Ga6	0.98	Ga6	0.94	Ga6	1.29
N7	−1.045	N7	−1.05	N7	−1.14	N7	−1.11	N7	−1.06	N7	−1.44
Ga8	0.99	Ga8	1.01	Al8	1.25	Al8	1.27	In8	1.10	In8	1.51
N9	−1.04	N9	−1.01	N9	−1.21	N9	−1.16	N9	−1.07	N9	−1.42
N10	−0.68	N10	−0.67	N10	−0.76	N10	−0.77	N10	−0.70	N10	−0.86
Ga11	1.00	Ga11	1.02	Ga11	0.99	Ga11	1.00	Ga11	0.97	Ga11	1.41
N12	−0.98	N12	−0.90	N12	−1.07	N12	−0.94	N12	−0.99	N12	−1.36
Ga13	0.92	Ga13	0.92	Al13	1.20	Al13	1.17	In13	1.02	In13	1.30
N14	−0.68	N14	−0.69	N14	−0.76	N14	−0.75	N14	−0.71	N14	−0.92
Ga15	1.00	Ga15	1.02	Ga15	1.00	Ga15	1.01	Ga15	0.98	Ga15	1.41
N16	−0.57	N16	−0.54	N16	−0.63	N16	−0.62	N16	−0.58	N16	−0.84
N17	−0.55	N17	−0.53	N17	−0.62	N17	−0.60	N17	−0.56	N17	−0.82
		H18	−0.03			H18	−0.03			H18	−0.07

tropic chemical-shielding (CSI) and anisotropic chemical-shielding (CSA) [84]:

$$\sigma_{iso} = (\sigma_{11} + \sigma_{22} + \sigma_{33})/3, \quad (10)$$

$$\sigma_{aniso} = \sigma_{33} - (\sigma_{22} + \sigma_{11})/2. \quad (11)$$

The NMR data of isotropic (σ_{iso}) and anisotropic shielding tensors (σ_{aniso}) for Mn-doped GaN, AlGaN and InGaN and their hydrated derivatives of Mn@GaN–H, Mn@AlGaN–H, Mn@InGaN–H have been computed by Gaussian 16 revision C.01 program package [61] and been shown in Table 2. The notable fragile signal intensity close to the parallel edge of the nanocluster sample might be owing to manganese binding induced non-spherical distribution of GaN (Fig. 6a) and Mn@AlGaN (Fig. 6b) heteroclusters. Figure 6c exhibited the same tendency of shielding; however, a considerable deviation exists from doping atoms of manganese as electron acceptors on the surface of Mn@InGaN heterocluster.

The observed increase in the chemical shift anisotropy spans for nanocages of Mn@GaN/ Mn@GaN–H (Fig. 6a) and Mn@InGaN/ Mn@InGaN–H (Fig.6c) is near N10 and N14, and for Mn@AlGaN/Mn@AlGaN–H is close to N10, N14, and N17 (Fig. 6b). The yield of electromagnetic shifting can be directed by the mentioned active nitrogen atoms extracted from hybrid nanomaterials. So, it can be observed that doped heteroclusters of Mn@GaN, Mn@AlGaN, or Mn@InGaN might ameliorate the capability of GaN-based nanocomposites for energy storage.

3.3. Insight of Infrared Spectroscopy and thermochemistry

The infrared spectroscopy (IR) has been performed for nanocomposites of Mn@GaN/ Mn@GaN–H (Figs. 7a, 7a'), Mn@AlGaN/ Mn@AlGaN–H (Figs. 7b, 7b'), and Mn@InGaN/ Mn@InGaN–H (Figs. 7c, 7c') through hydrogen adsorption. The frequency value through the IR curves between 200–1000 cm^{-1} for Mn@GaN with one sharp peak around 414.78 cm^{-1} (Fig. 7a) has been shifted to two pointed peaks around 863.78 and 921.24 cm^{-1} of Mn@GaN–H (Fig. 7a'). However, Fig. 7b shows two sharp peaks around 389.02 and 713.88 cm^{-1} for Mn@AlGaN that have been shifted to one sharp peak around 952.45 cm^{-1} for Mn@AlGaN–H (Fig. 7b'). Furthermore, Fig. 7c indicates one sharp peak around 366.88 cm^{-1} for Mn@InGaN that have been shifted to several sharp peaks around 640.30, 767.66, 783.92 and 1311.73 cm^{-1} for Mn@InGaN–H (Fig. 7c').

Energy storage with heteroclusters has described that the frame of the overcoming cluster is related to Mn@GaN–H, Mn@AlGaN–H, and Mn@InGaN–

Table 2. Data of NMR shielding tensors (ppm) for selected atoms of Si–AlGaN, Si–AlGaN–H, Ge–AlGaN, Ge–AlGaN–H, Pd–AlGaN, Pd–AlGaN–H, Pt–AlGaN, Pt–AlGaN–H heteroclusters

Mn@GaN			Mn@GaN–H			Mn@AlGaN		
atom	σ_{iso}	σ_{aniso}	atom	σ_{iso}	σ_{aniso}	atom	σ_{iso}	σ_{aniso}
Ga1	10.67	8.11	Ga1	7.81	31.27	Ga1	10.46	8.16
N2	127.83	150.77	N2	11.32	302.27	N2	146.57	121.34
Ga3	8.89	7.12	Ga3	0.04	103.91	Al3	7.35	7.05
N4	59.22	255.84	N4	518.43	1015.75	N4	89.08	176.73
Mn5	1103.19	682.75	Mn5	61898.62	83180.70	Mn5	860.19	607.87
Ga6	8.90	7.14	Ga6	2.09	109.30	Ga6	8.75	6.97
N7	128.15	149.77	N7	45.01	440.55	N7	146.58	115.60
Ga8	10.67	8.07	Ga8	5.62	31.70	Al8	9.14	9.24
N9	41.82	220.76	N9	445.69	929.93	N9	97.56	202.55
N10	1008.93	1461.38	N10	3715.85	8298.31	N10	1048.85	1558.03
Ga11	4.05	15.54	Ga11	0.25	102.04	Ga11	3.09	15.67
N12	120.72	362.25	N12	367.10	1288.90	N12	94.30	348.42
Ga13	2.27	25.19	Ga13	35.18	123.51	Al13	4.12	27.49
N14	1007.77	1458.05	N14	1857.11	7832.51	N14	1063.72	1562.00
Ga15	4.05	15.52	Ga15	11.51	73.33	Ga15	3.06	15.69
N16	120.67	305.81	N16	655.73	1345.89	N16	119.16	317.73
N17	180.86	320.66	N17	1055.92	1712.11	N17	171.08	325.89
–	–	–	H18	40.61	502.41	–	–	–
Mn@AlGaN –H			Mn@InGaN			Mn@InGaN –H		
atom	σ_{iso}	σ_{aniso}	atom	σ_{iso}	σ_{aniso}	atom	σ_{iso}	σ_{aniso}
Ga1	9.41	57.45	Ga1	9.85	9.07	Ga1	1.67	42.34
N2	523.29	1969.38	N2	141.28	139.24	N2	43.02	535.24
Al3	3.93	125.80	In3	10.62	6.08	In3	16.13	137.02
N4	1362.43	2433.13	N4	70.74	185.38	N4	1588.00	3484.48
Mn5	44890.87	68750.26	Mn5	1100.80	655.48	Mn5	75829.24	87460.28
Ga6	14.42	140.95	Ga6	8.06	6.49	Ga6	12.65	135.72
N7	367.17	1905.43	N7	138.27	141.26	N7	190.10	374.03
Al8	1.36	33.67	In8	11.51	8.96	In8	3.96	42.30
N9	1645.66	2817.25	N9	76.75	215.61	N9	105.91	687.93
N10	2093.50	9430.31	N10	1078.67	1612.40	N10	6052.66	10061.71
Ga11	33.24	113.47	Ga11	2.50	16.30	Ga11	52.05	69.72
N12	610.21	1774.94	N12	101.36	375.90	N12	883.03	2354.12
Al13	10.85	248.54	In13	0.69	25.46	In13	17.90	85.90
N14	3210.83	7998.79	N14	1134.38	1669.99	N14	11759.92	18294.74
Ga15	26.82	118.02	Ga15	1.96	16.69	Ga15	87.78	114.00
N16	336.50	1962.75	N16	129.69	346.19	N16	124.00	695.59
N17	498.32	5128.17	N17	189.09	365.81	N17	216.71	726.14
H18	26.27	347.02	–	–	–	H18	91.23	651.13

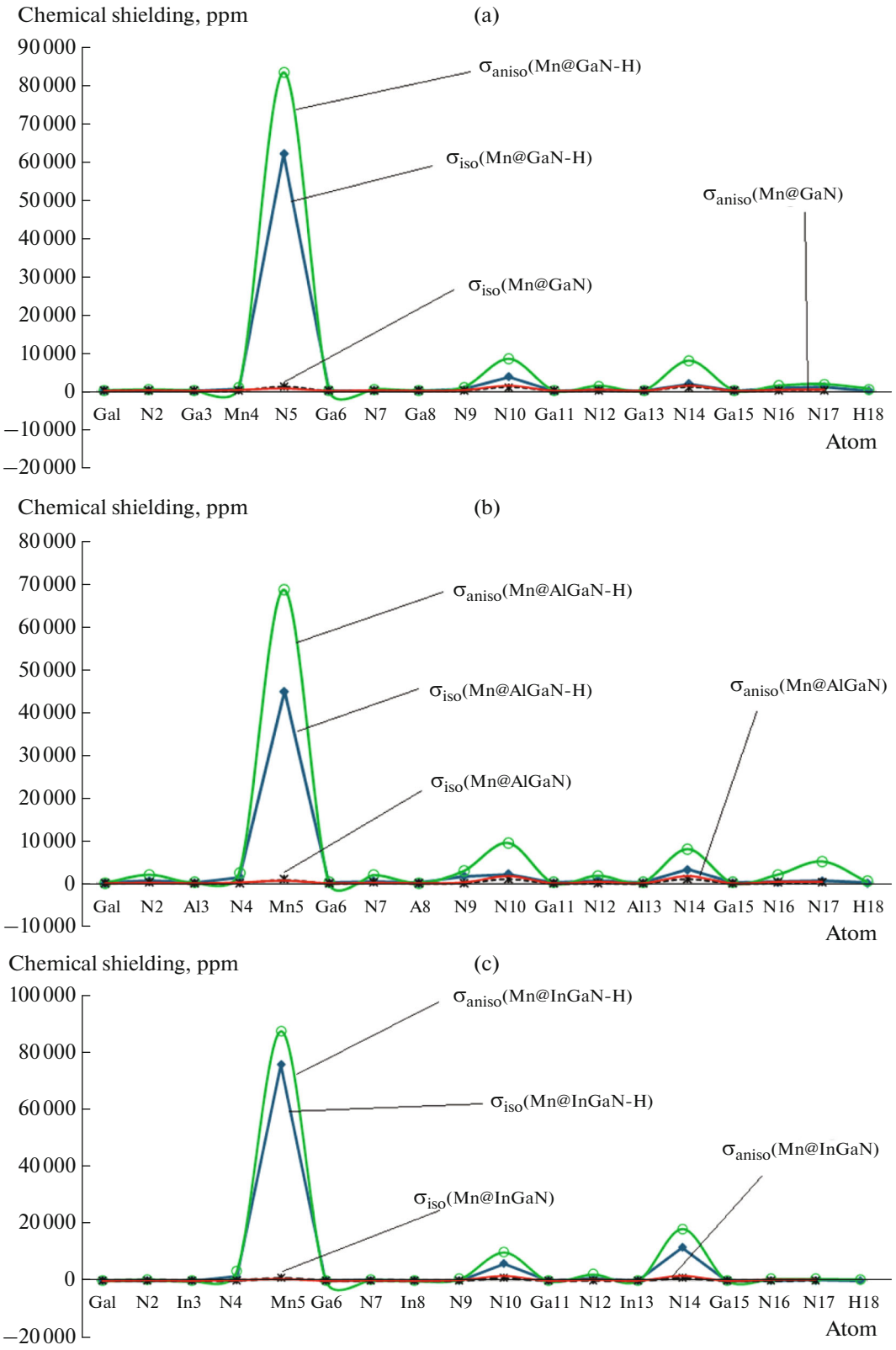

Fig. 6. The NMR spectra for heteroclusters of (a) Mn@GaN/Mn@GaN–H, (b) Mn@AlGaN/Mn@AlGaN–H, and (c) Mn@InGaN/Mn@InGaN–H.

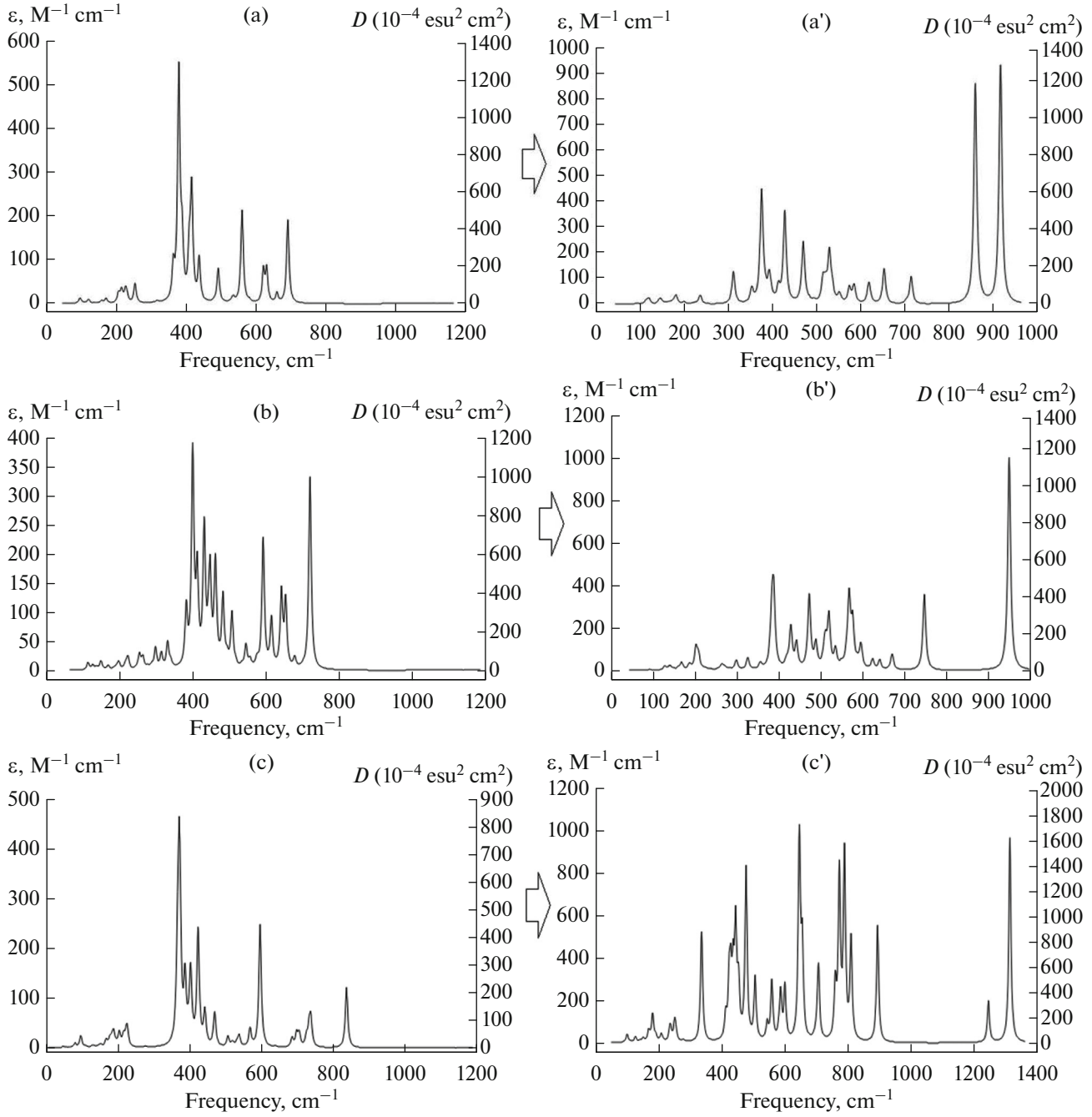

Fig. 7. The Frequency (cm^{-1}) changes through the IR spectra for heteroclusters of (a) Mn@GaN/Mn@GaN–H, (b) Mn@AlGaN/Mn@AlGaN–H, and (c) Mn@InGaN/Mn@InGaN–H.

H in the high amounts of frequency. This property makes these hybrid nanomaterials potentially advantageous for certain high-frequency applications for energy storage. The advantages of manganese over GaN, AlGaN, or InGaN include its higher electron and hole mobility, allowing manganese doping devices to operate at higher frequencies than non-doping devices.

Table 3 through the thermodynamic specifications concluded that heteroclusters of Mn@GaN, Mn@GaN–H, Mn@AlGaN, Mn@AlGaN–H, Mn@InGaN, Mn@InGaN–H might be more efficient structure for energy storage. Thermodynamic parameters of heteroclusters of Mn@GaN/Mn@GaN–H, Mn@AlGaN/Mn@AlGaN–H, and Mn@InGaN/Mn@InGaN–H have been assigned (Table 3). The changes of Gibbs

Table 3. The thermodynamic characters of Mn@GaN, Mn@GaN–H, Mn@AlGaN, Mn@AlGaN–H, Mn@InGaN, Mn@InGaN–H nanoclusters using CAM–B3LYP–D3/6–311+G(d,p) calculation

Compound	Dipole moment, D	$\Delta E^{o}_{ads} \times 10^{-3}$, kcal/mol	$\Delta H^{o}_{ads} \times 10^{-3}$, kcal/mol	$\Delta G^{o}_{ads} \times 10^{-3}$, kcal/mol	$\Delta E^{o}_{H\text{-binding}}$, kcal/mol
Mn@GaN	4.82	–383.44	–383.44	–383.48	–
Mn@GaN–H	7.37	–383.59	–383.59	–383.63	–157
Mn@AlGaN	4.79	–383.09	–383.09	–383.13	–
Mn@AlGaN–H	7.37	–383.59	–383.59	–383.63	–501
Mn@InGaN	7.36	–383.03	–383.03	–383.08	–
Mn@InGaN–H	4.30	–383.47	–383.47	–383.51	–437

free energy versus for all nanocomposites could detect the maximum efficiency of Mn@AlGaN–H > Mn@GaN–H > Mn@InGaN–H for energy storage through ΔG^{o}_{f}.

The adsorption efficiency of Mn@GaN–H, Mn@AlGaN–H, Mn@InGaN–H based on dipole moment has been evaluated by the ΔG^{o}_{f}. The semiconductors formed by Mn@GaN, Mn@AlGaN, Mn@InGaN feature a hierarchical structure with the electron donor/acceptor layer sandwiched by anode and cathode, which raises the importance of controlling the molecular crystal orientation, domain size, and vertical distribution to facilitate the charge collection at electrodes. In this paper, we have demonstrated that the nanocomposite semiconductor of gallium nitride-based structure can lead to a significant absorption enhancement in a broad spectral range of incident light in the presence of aluminum, indium and manganese. A comparison between semiconductors containing 3*d* transition metal of Mn-doped GaN, AlGaN, InGaN shows that a semiconductor containing these elements show a more enhanced cell performance than the cells containing only the bare gallium nitride-based structure. This efficient doping strategy not only bridges the gaps of heteroatom doped GaN-based semiconductor materials, but also can provide deep insights into controlling the electrical and optical properties of these doping hybrid nanoclusters.

CONCLUSIONS

We have provided gallium nitride-based semiconductors which are doped with manganese. The geometrical parameters of doping manganese on the surface of GaN, AlGaN, InGaN through the absorption status and current charge density was studied. Energy storage with heteroclusters has described that the frame of the overcoming cluster is related to Mn@GaN, Mn@AlGaN or Mn@InGaN in the high amounts of frequency. The changes of Gibbs free energy versus for all nanocomposites could detect the maximum efficiency of Mn@AlGaN–H > Mn@GaN–H > Mn@InGaN–H for energy storage through ΔG^{o}_{f}. The advantages of manganese over GaN, AlGaN, or InGaN include its higher electron and hole mobility, allowing manganese doping devices to operate at higher frequencies than non-doping devices. Thus, it should be explored its unique properties, such as its ability to increase energy storage which could lead to advancements semiconductors. The idea-based metal-doping might create a magnetic semiconductor involving GaN doped with Mn.

ACKNOWLEDGMENTS

In successfully completing this paper and its research, the authors are grateful to Kastamonu University.

FUNDING

This work was supported by ongoing institutional funding. No additional grants to carry out or direct this particular research were obtained.

CONFLICT OF INTEREST

The authors of this work declare that they have no conflicts of interest.

REFERENCES

1. I. S. Yakovenko and A. D. Kiverin, Russ. J. Phys. Chem. B **18**, 1069–1076 (2024). https://doi.org/10.1134/S1990793124700623
2. A. M. Tereza, G. L.Agafonov, E. K. Anderzhanov, et al., Russ. J. Phys. Chem. B **17**, 425–432 (2023). https://doi.org/10.1134/S1990793123020173

3. F. Mollaamin and M. Monajjemi, Russ. J. Phys. Chem. B **18**, 607–623 (2024). https://doi.org/10.1134/S1990793124020271
4. K. Y. Troshin, N. M. Rubtsov, G. I. Tsvetkov, et al., Russ. J. Phys. Chem. B **17**, 433–438 (2023). https://doi.org/10.1134/S1990793123020185
5. S. I. Sumskoi, A. S. Sof'in, S. K. Zainetdinov, et al., Russ. J. Phys. Chem. B **17**, 419–424 (2023). https://doi.org/10.1134/S199079312302015X
6. A. M. Tereza, G. L. Agafonov, E. K. Anderzhanov, et al., Russ. J. Phys. Chem. B **17**, 1294–1299 (2023). https://doi.org/10.1134/S1990793123060246
7. F. Mollaamin, Russ. J. Phys. Chem. B **18**, 805–820 (2024). https://doi.org/10.1134/S1990793124700131
8. S. Lv, S. Wang, T.Wang, et al., J. Mater. Chem. A **10**, 22007–22015 (2022). https://doi.org/10.1039/D2TA04540K
9. F. Mollaamin and M. Monajjemi, Russ. J. Phys. Chem. B **18**, 533–548 (2024). https://doi.org/10.1134/S199079312402012X
10. E. I. Rudenko, N. V. Dohlikova, A. K. Gatin, et al., Russ. J. Phys. Chem. B **17**, 845–852 (2023). https://doi.org/10.1134/S1990793123040164
11. A. E. Smygalina and A. D. Kiverin, Russ. J. Phys. Chem. B **18**, 1048–1059 (2024). https://doi.org/10.1134/S199079312470060X
12. V. V. Parakhin, V. M. Volokhov, E. S. Amosova, et al., Russ. J. Phys. Chem. B **18**, 697–706 (2024). https://doi.org/10.1134/S1990793124700088
13. F. Mollaamin and M. Monajjemi, J. Mol. Struct. **1300**, 137214 (2024). https://doi.org/10.1016/j.molstruc.2023.137214
14. A. A. Belyaev and B. S. Ermolaev, Russ. J. Phys. Chem. B **18**, 988–1001 (2024). https://doi.org/10.1134/S1990793124700532
15. A. M. Tereza, G. L. Agafonov, E. K. Anderzhanov, et al., Russ. J. Phys. Chem. B **18**, 965–972 (2024). https://doi.org/10.1134/S1990793124700416
16. C. Li, X. Chen, and Z. Wang, Micromachines **15**, 330 (2024). https://doi.org/10.3390/mi15030330
17. Z. Wang, J. Comput. Electron. **18**, 1251–1258 (2019). https://doi.org/10.1007/s10825-019-01383-7
18. Z. Wang, J. Cao, F. Wang, et al., Superlattices Microstruct. 122, 343–348 (2018). https://doi.org/10.1016/j.spmi.2018.07.016
19. S. Mishra, P. Kachhawa, P. Mondal, et al., IEEE Trans. Electron Devices **69**, 4527–4533 (2022). https://doi.org/10.1109/TED.2022.3184658
20. A. M. Bhat, C. Periasamy, R. Poonia, et al., IEEE Trans. Nanotechnol. **22**, 466–472 (2023). https://doi.org/10.1109/TNANO.2023.3305360
21. S. Liu, C. Ye, X. Cai, et al., Appl. Phys. A **122**, 527 (2016). https://doi.org/10.1007/s00339-016-0073-0
22. Z. Wang, Z. Zhang, S. Wang, et al., Appl. Sci. **9**, 3054 (2019). https://doi.org/10.3390/app9153054
23. T. M. Altahtamouni, J. Y. Lin, and H. X. Jiang, AIP Adv. **4**, 047122 (2014). https://doi.org/10.1063/1.4871996
24. J.-K. Sheu, P.-C. Chen, C.-L. Shin, et al., Sol. Energy Mater. Sol. Cells **157**, 727–732 (2016). https://doi.org/10.1016/j.solmat.2016.07.047
25. F. Mollaamin and M. Monajjemi, Russ. J. Phys. Chem. B **17**, 658–672 (2023). https://doi.org/10.1134/S1990793123030223
26. V. E. Khrapovskii, V. G. Khudaverdiev, A. A. Sulimov, et al., Russ. J. Phys. Chem. B **18**, 1060–1068 (2024). https://doi.org/10.1134/S1990793124700611
27. J.-K. Sheu, F.-W. Huang, C.-H. Lee, et al., Appl. Phys. Lett. **103**, 063906 (2013). https://doi.org/10.1063/1.4818340
28. A. Martí, C. Tablero, E. Antolín, et al., Sol. Energy Mater. Sol. Cells **93**, 641–644 (2009). https://doi.org/10.1016/j.solmat.2008.12.031
29. M. I. Ikim, E. Y. Spiridonova, V. F. Gromov, et al., Russ. J. Phys. Chem. B **17**, 774–777 (2023). https://doi.org/10.1134/S199079312303003X
30. J. Wu, W. Walukiewicz, K. M. Yu, et al., J Appl. Phys. **94**, 6477–6482 (2003). https://doi.org/10.1063/1.1618353
31. J. Wu, W. Walukiewicz, K. Yu, et al., Appl. Phys. Lett. **80**, 4741–4743 (2002). https://doi.org/10.1063/1.1489481
32. R. Singh, D. Doppalapudi, T. D. Moustakas, et al., Appl Phys Lett. **70**, 1089–1091 (1997). https://doi.org/10.1063/1.118493
33. D. H. Lien, Y. H. Hsiao, S. G. Yang, et al., Nano Energy **11**, 104–109 (2015). https://doi.org/10.1016/j.nanoen.2014.10.013
34. Y. Kuwahara, T. Fujii, Y. Fujiyama, et al., Appl Phys Express **3**, 111001 (2010). https://doi.org/10.1143/APEX.3.111001
35. N. G. Young, R. M. Farrell, Y. L. Hu, et al., Appl Phys Lett. **103**, 173903 (2013). https://doi.org/10.1063/1.4826483
36. C. J. Neufeld, S. C. Cruz, R. M. Farrell, et al., Appl Phys Lett. **98**, 243507 (2011). https://doi.org/10.1063/1.3595487
37. Sh. B. Utamuradova, D. A. Rakhmanov, P. L. Tuan, et al., Adv. Phys. Res. **6**, 83–89 (2024). https://doi.org/10.62476/apr62.83
38. K. X. Wang, Z. Yu, V. Liu, et al., Nano Lett. **12**, 1616–1619 (2012). https://doi.org/10.1021/nl204550q
39. A. F. Noori, A. M. Ghaleb, and A. I. Salih, Adv. Phys. Res. **6**, 225–238 (2024). https://doi.org/10.62476/apr63225
40. K. V. Zolotarev, A. N. Mikhailov, V. I. Nakhod, et al., New Mater., Compd. Appl. **8**, 162–170 (2024). https://doi.org/10.62476/nmca82162
41. Sh.B. Utamuradova, Sh.Kh. Daliev, B. R. Bokiev, et al., Advanced Physical Research. 6, 211–218 (2024). https://doi.org/10.62476/apr63211
42. A. F. Gochuyeva, A. M. Mehdiyeva, and S. V. Bakhshaliyeva, New Mater., Compd. Appl. **8**, 87–93 (2024). https://doi.org/10.62476/nmca8187

43. K. V. Zolotarev, A. N. Mikhailov, V. I. Nakhod, et al., New Mater., Compd. Appl. **8**, 162–170 (2024). https://doi.org/10.62476/nmca82162
44. J. Lin, Y. Yu, Z. Xu, et al., J. Power Sources **450**, 227578 (2020). https://doi.org/10.1016/j.jpowsour.2019.227578
45. U. K. Kumawat, K. Kumar, P. Bhardwaj, et al., Energy Sci. Eng. **7**, 2469–2482 (2019). https://doi.org/10.1002/ese3.436
46. F. Mollaamin, S. Shahriari, and M. Monajjemi, Russ. J. Phys. Chem. B 18, 398–418 (2024). https://doi.org/10.1134/S199079312402026X
47. S. Krishnamurthy, M. van Schilfgaarde, and N. Newman, Appl. Phys. Lett. 83, 1761–1763 (2003). https://doi.org/10.1063/1.1606873
48. A. V. Komarov, A. V. Los, S. M. Ryabchenko, and S. M. Romanenko, J. Appl. Phys. 109, 083936 (2011). https://doi.org/10.1063/1.3581142
49. N. Tandon, G. P. Das, A. Kshirsagar, J. Phys.: Condens. Matter **18**, 9245 (2006). https://doi.org/10.1088/0953-8984/18/40/010
50. F. Mollaamin and M. Monajjemi, Russ. J. Phys. Chem. B **18**, 1177–1198 (2024). https://doi.org/10.1134/S1990793124700507
51. H. K. Ismail, R. A. Omer, Y. H. Azeez, et al., Russ. J. Phys. Chem. B **18**, 1148–1165 (2024). https://doi.org/10.1134/S1990793124700477
52. F. Mollaamin and M. Monajjemi, Russ. J. Phys. Chem. B **18**, 1199–1216 (2024). https://doi.org/10.1134/S1990793124700519
53. A. G. Chetverikova, V. L. Berdinsky, O. N. Kanygina, et al., Russ. J. Phys. Chem. B **18**, 378–387 (2024). https://doi.org/10.1134/S1990793124020052
54. F. Mollaamin and M. Monajjemi, Russ. J. Phys. Chem. B **18**, 49–66 (2024). https://doi.org/10.1134/S1990793124010159
55. F. Mollaamin, S. Mohammadi, Z. Khalaj, et al., Russ. J. Phys. Chem. B **18**, 67–82 (2024). https://doi.org/10.1134/S1990793124010330
56. L. K. Abdullayeva and M. H. Hasanov, New Mater., Compd. Appl. **8**, 135–141(2024). https://doi.org/10.62476/nmca8135
57. F. Mollaamin and M. Monajjemi, Int. J. Quantum Chem. **124**, e27348 (2024). . https://doi.org/10.1002/qua.27348
58. Q. Q. Xiong, Russ. J. Phys. Chem. B **18**, 638–644 (2024). https://doi.org/10.1134/S1990793124700155
59. F. Mollaamin and M. Monajjemi, Mol. Simul. **49**, 365–376 (2023). https://doi.org/10.1080/08927022.2022.2159996
60. A. H. Davtyan, Z. O. Manukyan, S. D. Arsentev, et al., Russ. J. Phys. Chem. B **17**, 336–345 (2023). https://doi.org/10.1134/S1990793123020239
61. M. J. Frisch, G. W. Trucks, H. B. Schlegel, G. E. Scuseria, M. A. Robb, J. R. Cheeseman, G. Scalmani, V. Barone, G. A. Petersson, H. Nakatsuji, X. Li, M. Caricato, A. V. Marenich, J. Bloino, B. G. Janesko, R. Gomperts, B. Mennucci, H. P. Hratchian, J. V. Ortiz, A. F. Izmaylov, J. L. Sonnenberg, D. Williams-Young, F. Ding, F. Lipparini, F. Egidi, J. Goings, B. Peng, A. Petrone, T. Henderson, D. Ranasinghe, V. G. Zakrzewski, J. Gao, N. Rega, G. Zheng, W. Liang, M. Hada, M. Ehara, K. Toyota, R. Fukuda, J. Hasegawa, M. Ishida, T. Nakajima, Y. Honda, O. Kitao, H. Nakai, T. Vreven, K. Throssell, J. A. Montgomery, Jr., J. E. Peralta, F. Ogliaro, M. J. Bearpark, J. J. Heyd, E. N. Brothers, K. N. Kudin, V. N. Staroverov, T. A. Keith, R. Kobayashi, J. Normand, K. Raghavachari, A. P. Rendell, J. C. Burant, S. S. Iyengar, J. Tomasi, M. Cossi, J. M. Millam, M. Klene, C. Adamo, R. Cammi, J. W. Ochterski, R. L. Martin, K. Morokuma, O. Farkas, J. B. Foresman, and D. J. Fox, *Gaussian 16, Revision C.01* (Gaussian, Inc., Wallingford, CT, 2016).
62. R. Dennington, T. A. Keith, J. M. Millam, *GaussView, Version 6.06.16* (Semichem Inc., Shawnee Mission, KS, 2016).
63. Z. Xu, C. Qin, Y. Yu, et al., AIP Adv. **14**, 055114 (2024). https://doi.org/10.1063/5.0208082
64. A. D. Becke and K. E. Edgecombe, J. Chem. Phys. **9**, 5397–5403 (1990). https://doi.org/10.1063/1.458517
65. S. N. Steinmann, Y. Mob, and C. Corminboeuf, Phys. Chem. Chem. Phys. **13**, 20584–20592 (2011). https://doi.org/10.1039/C1CP21055F
66. L. Tian, C. Feiwu, W. Xuebao, Acta Phys. Chim. Sin. 27, 2786–2792 (2011). https://doi.org/10.3866/PKU.WHXB20112786
67. A. Savin, O. Jepsen, J. Flad, et al., Angew. Chem. Int. Edit. Engl. **31**, 187–188 (1992). https://doi.org/10.1002/anie.199201871
68. F. Mollaamin and M. Monajjemi, J. Mol. Model. **29**, 119 (2023). https://doi.org/10.1007/s00894-023-05526-3
69. K. Bakhshi, F. Mollaamin, and M. Monajjemi, J. Comput. Theor. Nanosci. **8**, 763–768 (2011). https://doi.org/10.1166/jctn.2011.1750
70. F. Mollaamin, S. Shahriari, M. Monajjemi, et al., J. Cluster Sci. **34**, 1547–1562 (2023). https://doi.org/10.1007/s10876-022-02335-1
71. M. Monajjemi, F. Mollaamin, S. Shahriari, et al., Russ. J. Phys. Chem. B **18**, 1090–1112 (2024). https://doi.org/10.1134/S1990793124700465
72. F. Mollaamin and M. Monajjemi, J. Cluster Sci. **34**, 2901–2918 (2023). https://doi.org/10.1007/s10876-023-02436-5
73. M. A. A. Zadeh, H. Lari, L. Kharghanian, et al., J. Comput. Theor. Nanosci. **12**, 4358 (2015). https://doi.org/10.1166/jctn.2015.4366
74. F. Mollaamin and M. Monajjemi, Sensor Rev. **43**, 266–279 (2023). https://doi.org/10.1108/SR-03-2023-0040
75. M. Monajjemi, A. Sobhanmanesh, and F. Mollaamin, Fullerenes, Nanotubes Carbon Nanostruct. **21**, 47–63 (2013). https://doi.org/10.1080/1536383X.2011.574325
76. F. Mollaamin and M. Monajjemi, C—J. Carbon Res. **9**, 20 (2023). https://doi.org/10.3390/c9010020
77. B. Khalili Hadad, F. Mollaamin, and M. Monajjemi, Russ. Chem. Bull. **60**, 238–241 (2011). https://doi.org/10.1007/s11172-011-0039-5

78. F. Mollaamin and M. Monajjemi, J. Bio- Tribo-Corros. **9**, 33 (2023).
https://doi.org/10.1007/s40735-023-00751-y

79. M. Monajjemi, F. Mollaamin, and S. Shojaei, Biointerface Res. Appl. Chem. **10**, 5575 (2020).
https://doi.org/10.33263/BRIAC103.575585

80. F. Mollaamin, J. Comput. Theor. Nanosci. **11**, 2393–2398 (2014).
https://doi.org/10.1166/jctn.2014.3653

81. M. Monajjemi, H. Yamola and F. Mollaamin, Fullerenes, Nanotubes Carbon Nanostruct. **22**, 595–603 (2014).
https://doi.org/10.1080/1536383X.2012.702163

82. F. Mollaamin and M. Monajjemi, Computation **11**, 108 (2023).
https://doi.org/10.3390/computation11060108

83. F. Mollaamin and M. Monajjemi, Comput. Theor. Chem. **1237**, 114646 (2024).
https://doi.org/10.1016/j.comptc.2024.114646

84. U. Sohail, F. Ullah, N. H. Binti Zainal Arfan, et al., Molecules **28**, 4060 (2023).
https://doi.org/10.3390/molecules28104060